

Article

Targeted Disruption of the MORG1 Gene in Mice Causes Embryonic Resorption in Early Phase of Development

Sophie Wulf ^{1,†}, Luisa Mizko ^{1,†}, Karl-Heinz Herrmann ², Marta Sánchez-Carbonell ³, Anja Urbach ³, Cornelius Lemke ⁴, Alexander Berndt ⁵, Ivonne Loeffler ^{1,*} and Gunter Wolf ^{1,‡}

- ¹ Department of Internal Medicine III, Jena University Hospital, 07747 Jena, Germany; gunter.wolf@med.uni-jena.de (G.W.)
- ² Medical Physics Group, Institute of Diagnostic and Interventional Radiology, Jena University Hospital, 07747 Jena, Germany; karl-heinz.herrmann@med.uni-jena.de
- ³ Department of Neurology, Jena University Hospital, 07747 Jena, Germany; anja.urbach@med.uni-jena.de (A.U.)
- ⁴ Institute for Anatomy I, Jena University Hospital, 07743 Jena, Germany; corneliuslemke@gmx.de
- ⁵ Institute of Forensic Medicine, Section Pathology, Jena University Hospital, 07743 Jena, Germany; alexander.berndt@med.uni-jena.de
- * Correspondence: ivonne.loeffler@med.uni-jena.de
- † These authors contributed equally to this work.
- ‡ These authors share senior authorship.

Abstract: The mitogen-activated protein kinase organizer 1 (MORG1) is a scaffold molecule for the ERK signaling pathway, but also binds to prolyl-hydroxylase 3 and modulates HIF α expression. To obtain further insight into the role of MORG1, knockout-mice were generated by homologous recombination. While *Morg1*^{+/-} mice developed normally without any apparent phenotype, there were no live-born *Morg1*^{-/-} knockout offspring, indicating embryonic lethality. The intrauterine death of *Morg1*^{-/-} embryos is caused by a severe failure to develop brain and other neuronal structures such as the spinal cord and a failure of chorioallantoic fusion. On E8.5, *Morg1*^{-/-} embryos showed severe underdevelopment and proliferative arrest as indicated by absence of Ki67 expression, impaired placental vascularization and altered phenotype of trophoblast giant cells. On E9.5, the malformed *Morg1*^{-/-} embryos showed defective turning into the final fetal position and widespread apoptosis in many structures. In the subsequent days, apoptosis and decomposition of embryonic tissue progressed, accompanied by a massive infiltration of inflammatory cells. Developmental aberrancies were accompanied by altered expression of HIF-1/2 α and VEGF-A and caspase-3 activation in embryos and extraembryonic tissues. In conclusion, the results suggest a multifactorial process that causes embryonic death in homozygous *Morg1* mutant mice, described here, to the best of our knowledge, for the first time.

Keywords: MAP kinase organizer protein 1; WDR83; WD-40 repeat domain 83; PHD3; ERK



Citation: Wulf, S.; Mizko, L.; Herrmann, Ka.; Sánchez-Carbonell, M.; Urbach, A.; Lemke, C.; Berndt, A.; Loeffler, I.; Wolf, G. Targeted Disruption of the MORG1 Gene in Mice Causes Embryonic Resorption in Early Phase of Development. *Biomolecules* **2023**, *13*, 1037. <https://doi.org/10.3390/biom13071037>

Academic Editor: Vladimir N. Uversky

Received: 25 April 2023

Revised: 7 June 2023

Accepted: 20 June 2023

Published: 24 June 2023



Copyright: © 2023 by the authors. Licensee MDPI, Basel, Switzerland. This article is an open access article distributed under the terms and conditions of the Creative Commons Attribution (CC BY) license (<https://creativecommons.org/licenses/by/4.0/>).

1. Introduction

Mitogen-activated protein kinase organizer 1 (MORG1), also known as WDR83, is composed of 315 amino acids and belongs to the WD-40 domain protein family, which function as adapters in different protein–protein or protein–DNA complexes [1]. The MORG1 gene was shown to be expressed in various tissues, including the heart, brain, kidney, testis and liver [2]. Over the past few years, MORG1 was identified in a wide variety of physiological signaling pathways as well as in diverse pathophysiological processes.

MORG1 was also characterized as a binding partner of the MP1 scaffold protein that facilitates the activation of MEK1 and extracellular signal-regulated kinase 1 (ERK1). MP1 binds to late endosomes via the adapter protein p14, regulating endosomal traffic, cell proliferation and tissue homeostasis during embryogenesis [3]. MORG1 also interacts

directly with different components of the mitogen-activated protein kinase (MAPK) cascade and stabilizes their assembly into an oligomeric complex. MORG1 selectively promotes the activation of ERK1/2 or modulates their activation depending on its intracellular concentration in response to various agonists [2].

In addition to its role in the MAPK pathway, MORG1 is involved in another major pathway, the hypoxia-inducible factor (HIF) signaling, that regulates adaptive responses under tissue hypoxia. Under hypoxic conditions, the labile alpha and stable beta subunit of the HIF molecule heterodimerize and form a functional complex. The complex then translocates into the nucleus, where it induces the transcription of various genes involved in angiogenesis, cell proliferation, apoptosis and glucose metabolism [4]. HIF-1 α causes upregulation of glycolytic genes, which are responsible for tissue metabolic adaptation to oxygen deprivation and anaerobic ATP synthesis [5], whereas HIF-2 α is critical for the improvement of oxygen supply to hypoxic regions/areas by inducing erythropoietin (EPO) and vascular endothelial growth factor (VEGF) [5,6]. Under normoxia, prolyl hydroxylases 1-3 (PHD1-3) catalyze the oxygen-dependent hydroxylation of HIF α subunits, triggering its proteasomal degradation. MORG1 is a stabilizer of PHD3 and, thus, causes enhanced degradation of HIF [7]. It was previously shown that suppression of MORG1 induces HIF-mediated reporter gene activity and increases the stability of HIF-1/2 α proteins [7].

Furthermore, MORG1 is involved in the formation of apicobasal polarity in epithelial cells, a key step in tissue development and organization [8,9]. Finally, in humans, MORG1 was identified as an associated protein in the spliceosome, which catalyzes the pre-mRNA splicing [10].

While examining renal ischemia/reperfusion injury in mice, we previously observed that heterozygous *Morg1*^{+/-} mice exhibited a stronger increase in HIF-1/2 α expression in the kidney, associated with higher serum EPO levels. Interestingly, these animals were partially protected and showed less renal inflammation in response to acute renal ischemia [11].

Further studies also pointed to a partial protection of *Morg1*^{+/-} kidneys against systemic hypoxia and renal injury as a late consequence of diabetes mellitus types 1 and 2 [6,12]. This renoprotection may result from MORG1-dependent alterations in lipid metabolism in the course of diabetic nephropathy [13].

All mentioned pre-clinical findings were obtained using heterozygous *Morg1*^{+/-} knockout mice, since no homozygous (-/-) knockout animals are born. Indeed, the homozygous *Morg1*^{-/-} knockout genotype is not yet characterized in detail; therefore, we reasoned that it could provide important clues as to the physiological function of MORG1 in tissue development and homeostasis. Here, we present a detailed study of *Morg1*^{-/-} embryos. We report, to the best of our knowledge, for the first time on the exact timing of embryonic lethality of *Morg1*^{-/-} knockout progeny, the characterization of initial malformations and altered signal transduction pathways in early embryonic development that are associated with early embryonic death. In addition, we provide information for using MRI investigations as an innovative tool to screen for embryonic abnormalities.

2. Materials and Methods

2.1. Construction of the Targeting Vector

A murine 129/Sv BAC genomic library was screened using murine *Morg1* specific primers to generate an 810 bp amplicon. Two clones were isolated, restriction mapped and partially sequenced. An 8.4 kb restriction endonuclease BamHI fragment was subcloned into a cloning vector. This fragment spanned the whole coding region of the *Morg1* gene. A positive selectable cassette was introduced at two NsiI sites to delete the first five exons and create the replacement vector p*Morg1*-KO. This cassette contained stop codons in all three frames, an internal ribosomal entry site (IRES), followed by the enhanced green fluorescent protein (EGFP) gene with a SV40 polyadenylation signal and a neomycin phosphotransferase gene (NEOr) with polyadenylation signal, under control of the mouse

phosphoglycerate kinase (PGK) promoter. A negative selection cassette containing the diphtheria toxin (DTA) was ligated to the 5' end of the construct.

Transfection of embryonic stem cells (ES), screening for homologous recombination and generation of *Morg1* knockout mice.

To obtain *Morg1* chimeric mice, the construct was linearized, then electroporated into ES and selected for resistance to geneticin (G418). The resistant ES clones were analyzed for homologous recombination at the 5' and 3' end by polymerase chain reaction (PCR). Positive identified clones were further screened for homologous recombination with the targeted vector.

The clones were injected into C57BL/6J blastocysts to obtain chimeric mice. Male chimeras were mated to C57BL/6J mice and offspring screened for transmission of the disrupted allele. The heterozygous mice were backcrossed for 8–10 generations into C57BL/6J mice. *Morg1*^{+/-} were intercrossed to characterize phenotypes of *Morg1* homozygous (-/-) knockout mice.

All animal experiments were approved by the Local Ethics Committee of Landesamt für Gesundheit und Verbraucherschutz Hamburg and were carried out in accordance with the German Animal Protection Law. The animals were housed in a pathogen-free facility with a 12 h light-dark cycle and raised on standard chow and water ad libitum. For all animal experiments, the ARRIVE guidelines 2.0 were followed.

2.2. MRI

For MRI examination, 4–5 implantation sites remained connected by the uterine horn. They were fixed in 4% paraformaldehyde overnight (o/n) and embedded in 1% low temperature melting agarose in a falcon to keep in place. The medium must not interfere with the imaging process, must be stable to heat and easy to remove after MRI. The position of the embryos in the falcon had to be as close to the CryoProbe coil as possible. The embedded embryos were stored at 4 °C before and after the examination.

The embryo samples were scanned on a 9.4T Bruker MRI system (Bruker GmbH, Ettlingen, Germany) using the 2 ch quadrature CryoProbe to optimize the signal. For imaging, two different T2 weighted spinecho sequences were used. First, a standard Bruker MSME sequence in 3D mode to achieve an isotropic resolution of 50 µm, acquiring 8 equidistant echoes starting at TE = 7.46 ms (deltaTE = 7.46 ms), repetition time was TR = 1200 ms and the total acquisition time TA = 8 h.

The second sequence was developed in house [14] using a RARE acquisition with variable Flipangles (varFlipRARE). The flipangles followed an introductory series to achieve a steady state at alpha = 30°, which was then slowly increased during the RARE echo train. This allowed a RARE factor of 61 for a highly efficient data acquisition, permitting an isotropic resolution of 37 µm at nominal TE = 78 ms and TR = 1500 ms, acquiring 12 averages within a total acquisition time of TA = 6 h 6 min. For these scan parameters, the varFlipRARE sequence showed a pronounced diffusion weighting, mostly suppressing the MRI signal from liquid water. After the MRI examination, the embryos were cleared from agarose, embedded in paraffin and sectioned as described in Section 2.4.

2.3. Genotyping

The material for DNA isolation was obtained in three different ways: from tail biopsies, Reichert's membrane or paraffin sections. For genotyping of adult mice, tail biopsies were used. If the embryos underwent preparation, a piece of the Reichert's membrane was removed and used for the isolation. The tail biopsies were digested o/n and the Reichert's membrane samples for 2 h in proteinase A at 56 °C and gentle shaking in the Thermomixer C (Eppendorf, Hamburg, Germany). After the first incubation, the temperature was raised to 70 °C for 30 min and DNA was isolated using the NucleoSpin Tissue kit (Macherey-Nagel, Düren, Germany).

The embryos, which were embedded in utero, were sectioned first. A piece of embryonic material was then scratched off the slide using a pipette tip and diluted in xylene.

The digestion and isolation were performed using the QIAamp DNA FFPE Tissue kit (QIAGEN, Venlo, The Netherlands).

Genotyping was performed by PCR using the Mastercycler gradient (Eppendorf, Hamburg, Germany) to detect the mutated (sense primer 5'-GGCAAGGGCCAGTCAGCCTGC-3'; antisense primer 5'-GCCTCTGTTCCACATACACTTCAT-3') and the wild-type alleles (sense primer 5'-GGCAAGGGCCAGTCAGCCTGC-3'; antisense primer 5'-GATAACGAGGCAACTTCATCCT-3'). The mastermix was composed of 10 µL GoTaq DNA Polymerase (Promega, Fitchburg, MA, USA), 1 µL of three different Morg1 primers and 4 µL or 7 µL of sample and nuclease-free water to a total of 20 µL. When DNA was isolated from paraffin sections, 7 µL of isolated DNA were used due to small tissue volume and subsequent low DNA amount in the sample. If the isolation was performed from tail biopsies or Reichert's membrane, only 4 µL of isolated DNA were used and 3 µL of nuclease-free water added. Afterwards, the gene segments were analyzed by gel electrophoresis in the PowerPac Basic (Bio-Rad Laboratories, Hercules, CA, USA). In the evaluation, the wild-type band appeared at 500 bp, the knockout band at 300 bp and in the heterozygote samples, both bands can be observed. The gels were examined at the G-Box F3 (Syngene, Bangalore, India).

2.4. Preparation, Fixation, Embedding, Sectioning

The whole preparation was performed in a Petri dish containing PBS on ice. The embryos were separated from the surrounding extraembryonic tissue, placed in individual Petri dishes and rinsed in PBS. The uterus and other extraembryonic tissue were then removed under a stereomicroscope using pointed tip tweezers. A piece of the Reichert's membrane was extracted for genotyping and stored at $-20\text{ }^{\circ}\text{C}$ until further processing. The embryos were then photographed and, subsequently, fixed according to different protocols.

The fixation was performed using 4% paraformaldehyde (PFA) solution (RotiHistofix; Carl Roth, Karlsruhe, Germany). The various organs of adult mice as well as the embryos, that were still in utero, were placed directly in a tissue cassette and fixed o/n. The extracted embryos were placed in the cap of an Eppendorf tube, which was wrapped in a tissue bag, and then placed in a tissue cassette. In that way, it was possible to prevent the embryos from being crushed directly in the bag or lost through the gaps in the cassette. For those embryos, the following PFA incubation times were applied: E8.5 = 1.5 h; E9.5 = 2 h.

After fixation, the organs and embryos were rinsed in tap water for 1 h. The paraffin wax embedding was performed using the automatic Tissue Processor Leica TP1020 (Leica Biosystems, Wetzlar, Germany). After the paraffinization, the samples were embedded in paraffin blocks (Wetzlar, Germany) and stored at $4\text{ }^{\circ}\text{C}$ until further sectioning.

The 4 µm thick tissue sections were prepared using the Automated Rotary Microtome (Leica Biosystems, Wetzlar, Germany) and dried o/n at $37\text{ }^{\circ}\text{C}$.

2.5. Immunohistochemistry, Immunofluorescence

In order to prepare the sections for further staining, deparaffinization and hydrogenation had to take place. For heat-induced epitope retrieval, the slides were placed in preheated citrate buffer, consisting of 8.2 mL sodium citrate, 1.8 mL citric acid and 90 mL dH₂O, and cooked in a steamer for 25 min. The slides were then briefly cooled in dH₂O and washed in PBS. Deactivation of endogenous peroxidases was carried out for 10 min in 3% hydrogen peroxide (H₂O₂) solution (Carl Roth, Karlsruhe, Germany) at room temperature (RT). The sections were then washed three times for 5 min in PBS while shaking.

The blocking of nonspecific binding sites was achieved by incubation in RotiBlock (Carl Roth, Karlsruhe, Germany) blocking solution for at least 1 h at RT. After removal of excess blocking solution, primary antibody incubation took place in a wet chamber o/n at $4\text{ }^{\circ}\text{C}$. The following primary antibodies were used: rabbit polyclonal anti-CD31 (epitope C-terminus aa 650; Abcam, Cambridge, UK), rabbit monoclonal anti-Ki67 (epitope C-terminus; Abcam, Cambridge, UK), rabbit polyclonal anti-Morg1 (Biotrend, Berlin, Germany), rabbit polyclonal anti-PHD3 (Invitrogen, Carlsbad, CA, USA), rabbit polyclonal anti-VEGF-A (Lifespan Biosciences, Seattle, WA, USA), goat polyclonal anti-HIF-1α

(epitope Arg575-Asn826; R&D Systems, Minneapolis, MN, USA) and goat polyclonal anti-HIF-2 α (epitope Ser542-Thr87; R&D Systems, Minneapolis, MN, USA). The following day, the slides were washed three times for 5 min in PBS while being shaken. The horseradish peroxidase (HRP) labeled rabbit anti-goat IgG and goat anti-rabbit IgG secondary antibodies (both Medac Diagnostics, Wedel, Germany) were diluted 1:500 in blocking solution and incubation took place in a wet chamber for 1 h at RT. After that, the slides were washed again in PBS in the same way as before. The ImmPACT NovaRED Substrate Kit (Vector Laboratories, Burlingame, CA, USA) was prepared according to the instructions. Incubation times varied between 3 and 10 min, depending on the intensity of the staining reaction. The slides were then washed again in PBS three times and the sections coverslipped using AquaTex (Merck Millipore, Burlington, MA, USA).

To ascertain the specificity of MORG1 antibody, different strategies were performed: (1) “negative tissue” control: staining of MORG1 knockout embryos; (2) “secondary antibody only” control: staining with buffer instead of primary antibody; (3) “isotype” control: staining with IgG control instead of primary antibody (see Figure S1).

For immunofluorescence, after deparaffinization, heat-induced epitope retrieval was performed by cooking the slides in preheated sodium citrate/citric acid buffer in a steamer for 15 min. The blocking of nonspecific binding sites was carried out for 1 h in blocking solution consisting of 5% BSA in PBS sterile. Primary rabbit anti-cleaved caspase-3 antibody (Cell Signaling, Leiden, The Netherlands) was diluted in blocking solution and incubated at 4 °C o/n in a wet chamber. The following day, the sections were washed three times for 10 min in PBS while being gently shaken and, subsequently, incubated in blocking solution for 30 min. The secondary goat anti-rabbit IgG antibody, labeled with DyLight594 (Vector Laboratories, Burlingame, CA, USA), was diluted 1:200 in blocking solution and incubated for 2 h at RT in a wet chamber. The sections were then washed in PBS three times for 10 min and incubated with DAPI (Sigma Aldrich, St. Louis, MI, USA) for 10 min at RT in a dilution of 1:2000 in PBS sterile. The final washing steps were carried out three times for ten minutes in a sterile filtrated solution of PBS and 0.1% TritonX-100 (Ferak Berlin, Berlin, Germany). Finally, the sections were coverslipped using Vectashield antifade mounting media (Vector Laboratories, Burlingame, CA, USA) and immediately examined.

2.6. Hematoxylin and Eosin Staining (H&E)

First, deparaffination in xylol for 15 min and rehydration took place, after which hematoxylin (Hemalaun Solution Acid acc. to Mayer; Carl Roth, Karlsruhe, Germany) staining for 5 min ensued. Following washing in tap water for 15 min, the slides were counterstained with eosin G (Carl Roth, Karlsruhe, Germany) for 5 min. The slides were covered using the xylene soluble mounting media Pertex (Meditate, Burgdorf, Germany) and the Automatic Cover Slipping Machine (Meditate, Burgdorf, Germany).

2.7. Microscopy

All sections from IHC, IF and H&E staining were examined at the ZEISS Axio Imager 2 (Carl Zeiss, Oberkochen, Germany) or with whole slide scanner Vectra[®] Polaris[™] (Akoya Bioscience, Menlo Park, CA, USA) to show whole embryos. The caspase-3 IF microscopy was performed using channels specific for AF594 and DAPI.

2.8. Multiplex Immunofluorescence Labeling (mIF) and Multispectral Imaging

For multiplex IF, 3 μ m thick 12.5-day old wild-type murine embryo FFPE sections were placed on IHC microscope slides and dried for 1 h at 65 °C before deparaffination. Then, deparaffination and fixation in 4% PFA solution (RotiHistofix; Carl Roth, Karlsruhe, Germany) took place. For mIF labeling, the Opal[™] 4-Color anti-Rabbit Manual IHC Kit plus Opal[™] 620 (Akoya Bioscience, Menlo Park, CA, USA) was used according to the manufacturer’s protocol. After verification of the optimal pH of the AR buffer during HIER method as well as the optimal dilution for each primary antibody in a monoplex IF staining, the optimal staining sequence was tested by trying different positions of the primary antibodies. For

multiplexing, the mandatory steps (HIER, blocking, incubation of the primary and secondary antibody, OPAL signal generation) were repeated for each primary antibody (rabbit polyclonal anti-Morg1 (Boster Biological Technology, Pleasanton, CA, USA); rabbit monoclonal anti-WT1 (epitope human WT1 aa 59–269; Invitrogen, Waltham, MA, USA); rabbit monoclonal Ki67 (Abcam, Cambridge, UK); rabbit monoclonal anti-CD31 (epitope total CD31; Cell Signaling Technology, Danvers, MA, USA)).

After a final heating cycle in AR buffer and staining with DAPI, the slides were mounted with ProLong™ Diamond Antifade Mountant. For imaging, the scanner Vectra® Polaris™ (Akoya Bioscience) was used, which created whole-slide scans. Afterwards, the software Phenochart™ was necessary to visualize the scan file and adapt the brightness and color of specific Opals™. This method allowed for simultaneous detection of distinct biomarkers in various tissues leading to spatial phenotyping of the sample.

The autofluorescence controls were performed by monoplex staining without primary antibody (see Figure S1).

Furthermore, using the simulated brightfield mode (Pathology Views™), it was possible to render single channels of the fluorescence images displaying them as simulated DAB/Hematoxylin images.

2.9. Whole Mount Staining

Following the preparation, the embryos were rinsed in ice cold PBS and fixed in a 4:1 methanol/dimethyl sulfoxide (DMSO) solution o/n at 4 °C. The following day, the embryos were incubated for 5 h in a 4:1:2 methanol/DMSO/30% H₂O₂ solution. The H₂O₂ was used again to block endogenous peroxidase activity. After that, the tissue could be dehydrated and stored in 100% methanol at –20 °C or the staining could continue.

In order to proceed with IHC staining, the embryos must first be rehydrated. This was carried out in descending alcohol concentrations of 75%, 50% and 25% for 5 min in each solution while gently rocking. The embryos were then incubated twice in 0.5% TritonX 100 (Ferak Berlin, Berlin, Germany) in PBS sterile for 30 min at RT to further permeabilize the tissue. Permeabilization of the embryos was necessary for the blocking solution and antibodies to penetrate the tissue sufficiently. The blocking of nonspecific binding sites was achieved by incubation in RotiBlock blocking solution containing 0.5% TritonX 100 (Ferak Berlin, Berlin, Germany) and 0.2% sodium azide (Carl Roth, Karlsruhe, Germany) at 4 °C o/n. The embryos were then washed twice for 10 min in blocking solution. Embryos were placed in a 2 mL Eppendorf tube with rabbit anti-MORG1 antibody (Biotrend, Köln, Germany) diluted 1:1000 in blocking solution containing 0.2% sodium azide (Carl Roth, Karlsruhe, Germany) and incubation took place at 4 °C for 24 h. The following day, the embryos were washed three times for 1 h in blocking solution containing 0.5% TritonX 100 (Ferak Berlin, Berlin, Germany) at RT. The embryos were then incubated with the HRP-labelled secondary anti-rabbit IgG antibody (Medac Diagnostics, Wedel, Germany), diluted 1:500 in blocking solution, at 4 °C o/n. Afterwards, they were washed three times for 1 h in blocking solution containing 0.5% TritonX 100 (Ferak Berlin, Berlin, Germany) at RT.

Embryos were incubated for 1 h in the DAB staining substrate solution (Vector Laboratories, Burlingame, CA, USA). Subsequently, 1 drop of H₂O₂ was added and incubated for another 10 min. The staining reaction was stopped by rinsing in PBS three times. The embryos were postfixed in a 2% PFA solution o/n at 4 °C. Finally, they were dehydrated in ascending alcohol series of PBS, 50% methanol, 80% methanol for 30 min each and stored in 100% methanol at –20 °C. Every incubation step in the protocol was performed under gentle shaking. The pictures of the embryos were taken with a digital camera.

2.10. Statement about Sample Size Estimate, Blinding and Statistics

The sample size is indicated in each figure caption. Embryo assay readouts were a matter of yes and no, and so, power analysis for sample size was not necessary. Blinding was ensured, as genotyping was performed after the analyses. No statistical methods were used.

3. Results and Discussion

3.1. Spatial Expression Pattern of MORG1 Protein in Organs of Adult and Embryonic Mice

A search in the human protein atlas (<https://www.proteinatlas.org/ENSG00000123154-WDR83/tissue>; accessed on 2 July 2022) revealed that MORG1 (WDR83) protein is expressed at varying levels in almost all human organs and tissue systems. For example, in the brain, glial cells of the basal ganglia, hippocampal formation and cerebral cortex express MORG1 weakly, while Purkinje cells of the cerebellum expressed it moderately strong. Similarly, lung cells, liver cells, cardiomyocytes and tubule cells of the kidney were reported to express MORG1 moderately, while cells of the pancreas showed weak expression. In this study, immunohistological staining for MORG1 confirmed, for the first time, a widespread expression also in murine tissues (Figure 1A). Expression of MORG1 can be observed in brain, lung, kidney, heart, liver and pancreas tissue of adult mice. Glial cells, cardiomyocytes, islet cells of pancreas and proximal tubule cells of the kidney showed especially intense staining, whereas murine liver cells express MORG1 weakly.

To investigate the spatial expression of MORG1 in mouse embryos, whole-mount staining as well as IHC staining of paraffin sections for MORG1 on E12.5 wild-type embryo was performed (Figure 1B–D). In the whole mount staining, an intense staining of the neural tissue in the brain ventricles and developing organs could be observed and the liquid-filled ventricles were clearly visible in the embryos. There was no expression of MORG1 observed in the limbs (Figure 1B). In stained tissue sections, MORG1-immunoreactivity was detected in all developing organs (Figure 1C). Very high level of MORG1 expression was found in the neuroepithelium of the neural tube as well as in the trigeminal and dorsal root ganglia (Figure 1D). In addition to neuronal structures, the otic cavity and tail were also strongly positive. Intense staining was also observed in extraembryonic tissues, including in trophoblast cells (Figure 1C,D). In contrast to shown IHC of adult organs, MORG1 expression appeared stronger in liver cells and weaker in heart cells (compare Figure 1C with Figure 1A).

To obtain further evidence, whether MORG1 may be associated with proliferation and differentiation programs, we co-stained for Ki67 or WT1 (Figure 2). Ki67 is widely used as a proliferation marker. Although it is now clear that Ki67 is not required for proliferation, it was, nevertheless, highly expressed in cells undergoing mitosis [15]. The Wilms' tumor suppressor gene 1 (Wt1) was critically involved in a number of developmental processes in vertebrates, including cell differentiation, control of the epithelial/mesenchymal phenotype, proliferation and apoptosis [16]. As expected, the expressions of proliferation and differentiation markers Ki67 and WT1 did not overlap (Figure 2B–D). Furthermore, Ki67-positive cells were mainly found in the top layer of the neuroepithelium, endothelium and liver and WT1-positive cells mainly in the decidua, epicardium of the heart and the liver mesothelium (Figure 2B–D). In the literature, it was reported that Wt1 expression in the heart was predominantly, but not exclusively, associated with epicardial development. The earliest expression of Wt1 during cardiac morphogenesis was detected in mouse embryos at E9.5 in the proepicardium, which was the epicardial primordium; subsequently, Wt1 expression continues during the epicardial covering of the heart [16]. Wt1 was expressed in the liver mesothelium from the early stages of hepatic development. Liver mesothelial cells continued to express Wt1 when they migrated from the surface and intermingled with the hepatoblasts and the hematopoietic cells to differentiate into sinusoidal endothelium and stellate cells [16]. We observed partial colocalization of Ki67- and MORG1-positive cells (Figure 2E). Colocalization was particularly evident in the neuroepithelium and liver. Ki67-positive cells that did not express MORG1 were mainly found in the endothelia. In contrast to Ki67 staining, WT1-positive cells did not show any MORG1 co-expression (Figure 2F). These data supported a role of MORG1 in actively proliferating cells but not in cellular differentiation processes.

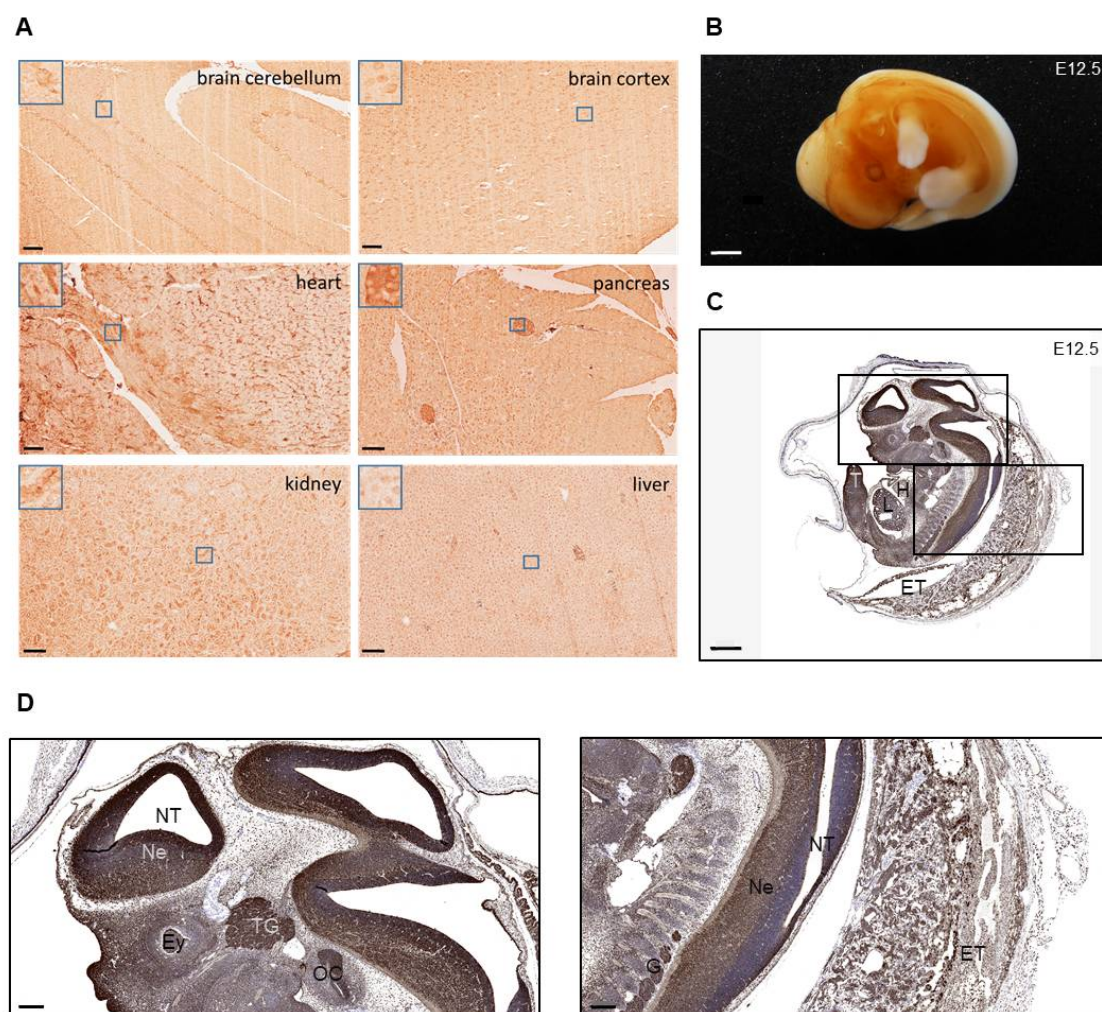


Figure 1. Immunohistochemical MORG1 staining of *Morg1*^{+/+} adult tissue and embryos. E = embryonic day; ET = extraembryonic tissue, Ey = eye; H = heart; L = liver; Ne = neuroepithelium; NT = neural tube; OC = otic cavity; T = tail; TG = trigeminal ganglion. (A) Staining of adult wild-type murine tissues showing the distribution of MORG1. MORG1 positive cells in brain cerebellum and cortex, in cardiomyocytes in heart, islets in pancreas, hepatocytes and proximal tubules in kidney. Scale bar = 100 μ m (B) MORG1 whole mount staining of *Morg1*^{+/+} embryo on E12.5. N = 2. Scale bar = 800 μ m (C,D) Simulated DAB/Hematoxylin image (Pathology Views™) from immunofluorescence of MORG1 on E12.5. (C) Particularly high expression in neuroepithelium of the neural tube and brain vesicles, ganglia and organ primordia. Scale bar = 800 μ m (D) Left picture displaying embryonic neural tissue with high expression of MORG1 in neuroepithelium, the trigeminal ganglion and otic cavity. Right picture showing neural tube and extraembryonic tissues with high expression in ganglia. Scale bar = 200 μ m.

To explore MORG1 distribution earlier in development, we resorted to publicly available datasets. The EMBL-EBI database (<https://www.ebi.ac.uk/gxa/genes/ensmusg0000005150>; accessed on 5 June 2023) documented MORG1 expression as early as E8.0 in trophoblast cells. According to the eGastrulation database (egastrulation.sibcb.ac.cn), MORG1 expression is widespread across embryonic tissues between days E5.5 and E7.5, with a particularly high expression in the ectodermal layer (from which, among other things, the central nervous system develops) (Figure S2).

In summary, we concluded that MORG1 exhibits broad embryonic tissue distribution in mice, similar to data reported in humans, with a particular high expression in the neuronal system.

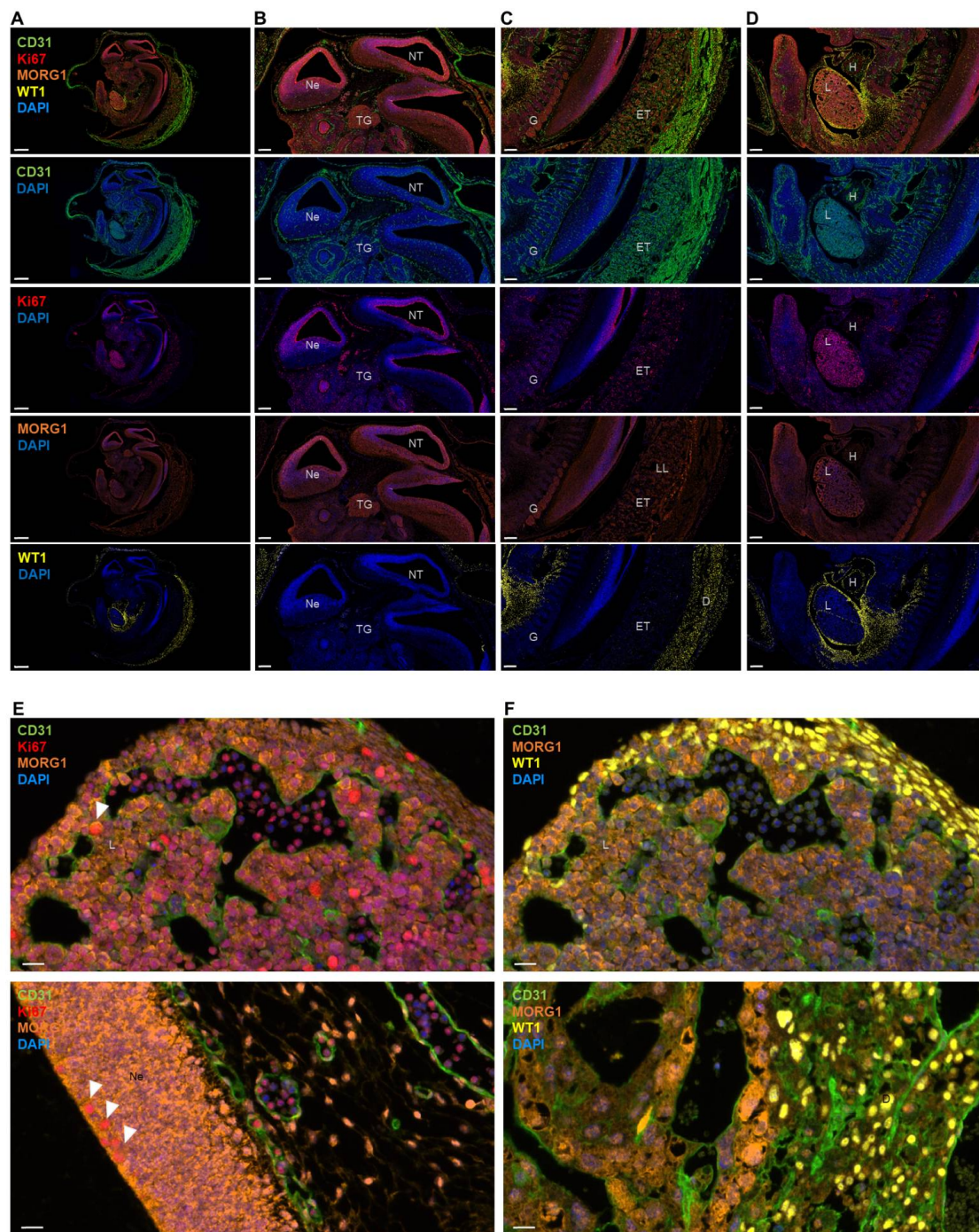


Figure 2. 4-plex immunofluorescence with CD31, Ki67, MORG1 and WT1 of MORG1^{+/+} E12.5 mouse embryo. D = decidua; E = embryonic day; ET = extraembryonic tissue, H = heart; L = liver; LL = labyrinth layer; Ne = neuroepithelium; NT = neural tube; TG = trigeminal ganglion. (A) Image of the whole embryo with combined and single antibody staining shown. Scale bar = 800 μ m (B) Image of the embryonic neural tissue. The vascular marker CD31 is highly expressed in vessel endothelium. Ki67 is detected in dividing cells in the top layer of the neuroepithelium of the embryo. MORG1 is expressed in many tissues like the neuroepithelium and the trigeminal ganglion. No expression of WT1 in the neuroectoderm was found. Scale bar = 200 μ m (C) Tissues surrounding the embryo shown. CD31 was detected in the highly vascularized extraembryonic tissue, while there was only few mitoses shown with Ki67. MORG1 is expressed extensively in the ganglia and the labyrinth layer of the placenta. Scale bar = 200 μ m (D) Throughout the mid-section of the embryo, particularly in the developing liver, CD31 was detected where Ki67 is also most abundant. A stronger expression of MORG1 could be found in

the liver than in the heart of the embryo. Contrasting MORG1, WT1 is mainly expressed in the mesothelial epithelium lining coelomic cavities. It can be found in the epicardium of the heart and the liver mesothelium. Scale bar = 200 μm (E) Ki67 seems to partially colocalize with MORG1 (white arrows). Colocalization was particularly evident in the liver (upper panel) and neuroepithelium (lower panel). Scale bars = 20 μm (F) WT1 shows no colocalization with MORG1, neither in the liver (upper panel) nor in the decidua (lower panel). Scale bars = 20 μm .

3.2. Generation of *Morg1* Knockout Mice and Characterization of Offspring

MORG1 was identified in a wide variety of physiological signaling pathways and pathological processes and, therefore, represents an interesting target in biomedical research. *Morg1* knockout mice were generated by homologous recombination [17]. *Morg1* was disrupted by a construct shown in Figure 3A. Genomic DNA was obtained from tail biopsies and genotyping was performed by PCR to detect the mutated and the wild-type alleles (Figure 3B). Heterozygous (+/−) mice were fertile and had no apparent phenotypes when compared to the wild-type (+/+) littermates.

Long-term observation revealed that *Morg1*+/- mice showed normal development of both sexes, and the oldest mice survived beyond 25 months of age without evidence of significant spontaneous disease. There were also no differences between heterozygous and wild-type mice in the different age groups regarding body weight (own observations).

3.3. Homozygous *Morg1* Knockout in Mice Leads to Embryonic Lethality

Morg1+/- were intercrossed to characterize phenotypes of *Morg1* homozygous (-/-) knockout mice. We monitored several generations and found that approximately 65% of the offspring were *Morg1*+/- and 35% were *Morg1*+/+ (Table 1). Yet, we never detected live-born *Morg1*-/- offspring, indicating that homozygous deletion of *Morg1* leads to embryonic lethality in mice. To further determine the developmental stage of embryonic death, the genotypes of embryos from embryonic days E8.5 to E12.5 from *Morg1*+/- intercrosses were analyzed (Table 1).

Table 1. Genotype analysis of offspring from *Morg1*+/- intercrosses. Numbers indicate observed embryos or born mice (in %) of each genotype at different stages of gestation. Expected percentage, based on Mendelian ratio 1:2:1, are in parentheses.

Embryonic Day	Total	<i>Morg1</i> Genotype			Unknown
		+/+	+/-	-/-	
E8.5	29	27.6% (25%)	44.9% (50%)	24.1% (25%)	3.4% *
E9.5	67	20.9% (25%)	46.3% (50%)	31.3% (25%)	1.5% *
E10.5	155	31.6% (25%)	46.5% (50%)	21.9% (25%)	0%
E11.5	80	26.3% (25%)	53.7% (50%)	0% (25%)	20% *
E12.5	38	23.7% (25%)	55.3% (50%)	0% (25%)	21% *
postnatal	75	34.7% (25%)	65.3% (50%)	0% (25%)	0%

* Unambiguous: genotyping was not possible in these embryos due to lack of material.

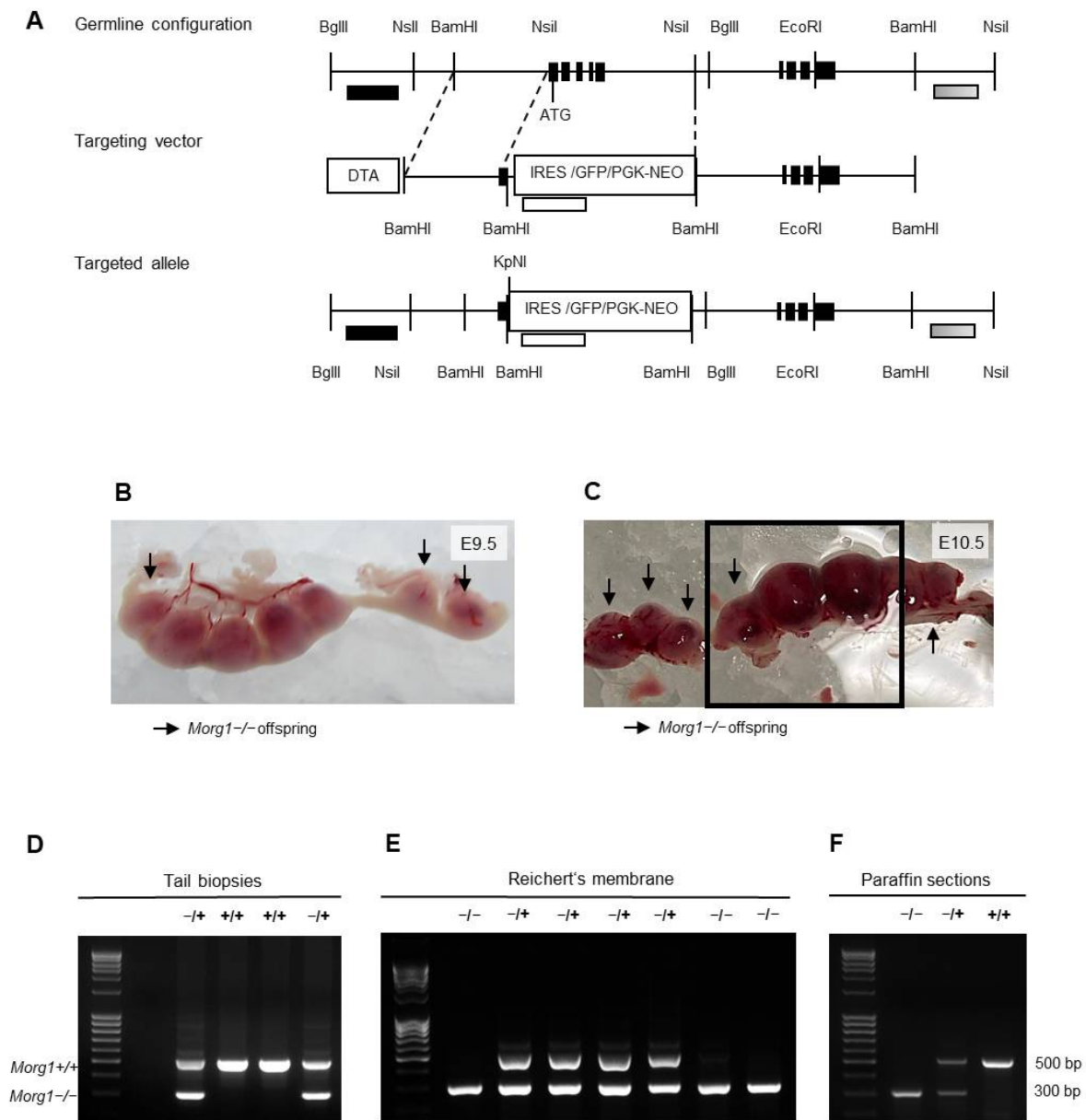


Figure 3. Generation of *Morg1*^{-/+} mice and *Morg1*^{-/-} embryos and genotyping of offspring. bp = base pair; DTA = diphtheria toxin; E = embryonic day; GFP = green fluorescence protein; IRES = internal ribosomal entry site; NEO = neomycin phosphotransferase; PGK = phosphoglycerate kinase. (A) Structure of *Morg1* knockout construct. Schematic illustration of germline configuration, targeting vector and targeted allele shown. (B) Genotyping results of adult mice using material obtained from tail biopsies. Only wild-type (*Morg1*^{+/+}) and heterozygous (*Morg1*^{-/+}) mice were born alive. (C,D) Genotyping results of embryos using material obtained from Reichert’s membrane (C) or paraffin sections (D). Homozygous knockout (*Morg1*^{-/-}) embryos were identified in addition to wild-type (*Morg1*^{+/+}) and heterozygous (*Morg1*^{-/+}) genotypes. (E,F) Uteri extracted on E9.5 and E10.5 from *Morg1*^{-/+} intercrosses. Implantation sites containing *Morg1*^{-/-} embryos (arrow) appear smaller and hemorrhagic on E10.5. Of note, the genotypings in C and D correspond to embryos from E and F in the same order.

Genotyping embryos at very early stages is challenging because no material from the embryos should be lost before the studies and contamination with maternal tissue must be avoided. To address both reservations, different methods were used in this study. The examination of embryonic tissue from paraffin sections as well as Reichert’s membrane

in early gestation revealed the presence of *Morg1*^{-/-} embryos (Figure 3C,D). From E8.5 to E10.5, *Morg1*^{-/-} embryos were seen at the expected frequency of a single-gene inheritance model (Mendelian distribution of 1:2:1). On E11.5 and E12.5, only embryos with the genotypes *Morg1*^{+/+} and *Morg1*^{+/-} could be unambiguously identified, since all other embryos found were already dead in utero. On E11.5 20% and on E12.5 21% of the litters, resorptions could be identified. There was a lack of material to genotype the embryonic residues unambiguously due to the advanced stage of resorption. Regarding the altered distribution of the genotypes after E10.5, we assumed that these embryos were likely *Morg1*^{-/-}. These results indicate that embryonic lethality of *Morg1*^{-/-} progeny occurred already in the first half of pregnancy prior to E11.5 leading to resorption in the mid-gestational stage. This was not unusual, because although conventional knockout mice are suitable genetic models for inherited diseases, they often exhibit embryonic or early postnatal lethality [18]. Approximately 25–30% of complete gene knockouts in mice cause intra-uterine lethality [19].

Our macroscopic examination of implantation sites of *Morg1*^{+/-} intercrosses identified an underdevelopment of *Morg1*^{-/-} embryos from E9.5 onwards and advanced resorption from E11.5. On E8.5, no macroscopic differences between the genotypes could be seen. All the implantation sites showed a physiological appearance and did not differ in size, color or shape (own observations). Already on E9.5, macroscopic differences between the genotypes could be seen: the *Morg1*^{-/-} embryos were clearly smaller (Figure 3E). On E10.5, the implantation sites occupied with *Morg1*^{-/-} embryos were significantly smaller than their healthy littermates and featured hemorrhages, as identified by the dark coloring (Figure 3F). Until E11.5, some continued to shrink and blood seemed to leak and accumulate further in the implantation sites, and on E12.5, only small dark resorption sites remained as a sign of aborted pregnancy (own observations). Due to the high proportion of resorptions and the fact that no more knockout embryos could be detected after E10.5, we assumed that the resorbed sites contained *Morg1*^{-/-} embryos.

3.4. Resorption of Embryonic Tissue on E12.5 and E11.5 as Well as Apoptosis and Decomposition of Embryos on E10.5 and E9.5 in the Morg1^{-/-} Genotype

The first indication of prenatal lethality is a deviating Mendelian distribution between the genotypes of heterozygous intercrosses, accompanied by a smaller litter size compared to control groups. If there is evidence that no viable homozygous offspring are born, the investigation of key stages of gestation is recommended [20]. Examination of a litter on E12.5 provides a good initial point in time. If there are implantation sites or embryonic residues detectable, the offspring died after implantation on E4.5. From the progression of resorption, the approximate time of death can then be deduced.

At E12.5, healthy wild-type embryos were approximately 7–9 mm in size and their organs were already present and continue to differentiate into functional units. In contrast, the resorption of the potential *Morg1*^{-/-} embryo and most of the surrounding tissue was already completed at this time-point (own observations). Only fragments of the extraembryonic tissue, such as the ruptured Reichert's membrane, could be identified in the former embryonic cavity. The resorption was characterized by massive evasion and clotting of maternal blood. The hemorrhagic blood clot contained numerous immune cells and was interspersed with fibrous material. Only at the edge of the dissolved or liquefied placental tissue decidual tissue was detectable. The extensive areas of infiltrating immune cells were surrounded by fibrinoid material, cell debris and mucus.

About 21% of E12.5 and 20% of E11.5 embryos were in a state of advanced resorption. Due to the previous apoptosis, infiltration and decomposition of *Morg1*^{-/-} embryos, it was assumed that they underwent degradation and subsequent resorption between E10.5 and E11.5. On E11.5, the physiologically developed embryos measured around 6–7 mm and all organs were already present in their primary structure. No such structures could be identified during the examination of the small and darkly colored *Morg1*^{-/-} embryos on E11.5 (own observations). While the uterine epithelium, spongial and labyrinth layer

were still visible, the embryonic tissue was already resorbed. However, the extraembryonic tissue displayed numerous apoptotic figures and underwent cytolysis. Extensive hemorrhages, consisting of erythrocytes and a high proportion of immune cells, were formed by bleeding from maternal vessels. Eosinophiles, which are involved in degradation of fibrous tissue, were particularly prominent in these areas. Massive accumulation of granulocytes populated the fading and disintegrating tissue and formed a purulent focus in the former embryonic cavity. Isolated shrunken apoptotic cells could be spotted between the necrotic tissue containing purulent debris.

In contrast, *Morg1*^{-/-} embryos were still detectable in the uterine cavity at E10.5, albeit much smaller compared to the wild type *Morg1*^{+/+}. However, infiltration of inflammatory cells and destruction of embryonic tissue was already evident (Figure 4A).

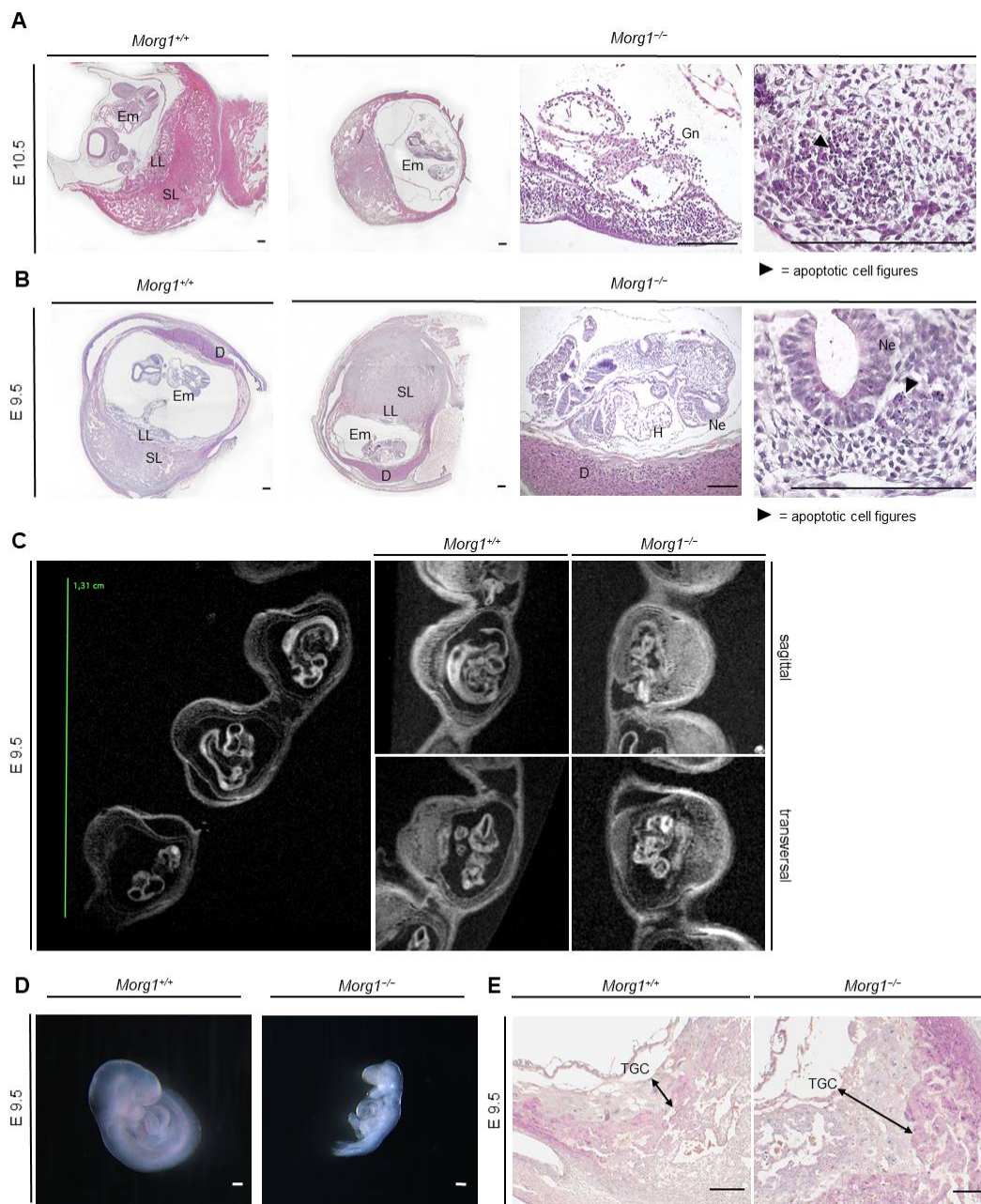


Figure 4. Apoptosis and decomposition of *Morg1*^{-/-} embryos. H&E staining. D = decidua; E = embryonic day; Em = embryo; Gn = granulocytes; H = heart; LL = labyrinth layer; Ne = neuroepithelium; SL = spongy layer; TGC = trophoblast giant cell. Scale bar = 200 μ m. (A) Decomposition of *Morg1*^{-/-} embryo

on E10.5 compared to healthy *Morg1*^{+/+} embryo. *Morg1*^{-/-} embryo displays apoptosis, loose cellular structure and massive infiltration of immune cells. The maternal moiety of the implantation site seems intact. N = 3 each of wild-type and knockout. (B) Underdeveloped *Morg1*^{-/-} embryo is smaller than the healthy *Morg1*^{+/+} embryo and exhibits defective turning into the final fetal position and failure of chorioallantoic fusion. The *Morg1*^{-/-} embryo is in an early stage of apoptosis, displaying nuclear fragmentation, loose cell cluster and cellular gaps, especially in the neuroepithelium. N = 3 each of wild-type and knockout. (C) Representative MRI images of *Morg1*^{+/+} and *Morg1*^{-/-} embryos together as implantation sites in the uteri (large image, on the left) or single in sagittal and transversal layer (small image, on the right). *Morg1*^{-/-} embryo exhibits growth retardation, advanced malformations and unstructured tissue appearance on E9.5. N = 9 (of which 2 knockout). (D) Stereomicroscopic images of unprocessed *Morg1*^{+/+} and *Morg1*^{-/-} embryos of the same litter. *Morg1*^{-/-} embryos are underdeveloped, much smaller and lack developmental features. The embryos failed to turn in curved embryonic position. N = 10 (of which 3 knockout). (E) H&E staining of extraembryonic tissue. *Morg1*^{-/-} placenta exhibits extended layer of TGCs on E9.5 and shows impaired vascularization including diminished formation of vascular beds. N = 3.

The mutant placenta took up less space but there was no evidence of cell death or excessive infiltration at this time (Figure 4A). The maternal moiety of the implantation site appeared intact. The embryos, on the other hand, were at a stage of late apoptosis, identified by nuclear fragmentation, and showed a loose and irregular cell association with barely differentiable tissue structures (Figure 4A). The embryonic cavity and embryo itself were extensively infiltrated by various immune cells, especially granulocytes, which was accompanied by tissue decomposition. The neuroepithelium of the degenerating embryo was irregular and showed large gaps in cell structure compared to the wild-type *Morg1*^{+/+} (Figure 4A). No organs were discernible due to impaired development and autolysis.

At E9.5, *Morg1*^{-/-} embryos were significantly smaller than their healthy littermates and featured a defective turning into the final fetal position, already pointing to underdevelopment (Figure 4B). The formation of organ primordia had progressed poorly and the embryos were already in an early stage of apoptosis, displaying nuclear fragmentation and cellular gaps. The neuroepithelium especially showed extended intracellular spaces with sporadic bleb forming.

3.5. Growth Retardation and Maldevelopment of *Morg1*^{-/-} Embryos on E9.5 and E8.5

Since the decomposition of the embryos was well advanced by day 10.5, we examined earlier stages to understand the underlying malformations by ex vivo MRI. In T2 weighted images, liquid water would usually be displayed very bright and other tissue in various shades of gray. However, the diffusion weighting due to the varFlipRARE sequence almost completely suppresses the signal from liquid water and creates a strong contrast to all other tissues. Using the medical image viewer OsiriX, the embryos could be rotated and viewed around all axes. Figure 4C shows representative images of *Morg1*^{+/+} and *Morg1*^{-/-} embryos on E9.5. *Morg1*^{+/+} embryos turned in the final fetal position where the back was facing the membranes surrounding the embryo. Organ primordia and brain ventricles were visible in the sagittal plane. In the transversal orientation, a closed neural tube and the primordia of the limbs could be seen. *Morg1*^{-/-} embryos appeared smaller and the tissue was unstructured and dissolved. In the sagittal plane, the embryonic vesicle was disrupted and embryonic tissue seemed to be moving out of the embryonic cavity (Figure 4C).

Stereomicroscopic images of extracted *Morg1*^{-/-} embryos also showed malformation on E9.5 compared to the wild-types (Figure 4D). At E9.5, no brain ventricles were visible in *Morg1*^{-/-} embryos, they exhibited a profound reduced tissue mass and lacked the physiologically curved embryonic position and failure of chorioallantoic fusion. Of note, there are several other examples of KO mice with failed chorioallantoic fusion in this embryonic development window of lethality [21,22]. In contrast to *Morg1*^{+/+} embryos, where several vessels and especially the aorta dorsalis could be seen immediately ventral to the somites, the formation of large vessels was poor or even absent in *Morg1*^{-/-},

indicating impaired vascularization. Another abnormality observed on E9.5 was a very prominent layer of TGCs surrounding the *Morg1*^{-/-} embryos, occupying significantly more placental space than in healthy offspring (Figure 4E).

Even at E8.5, *Morg1*^{-/-} embryos showed growth inhibition and advanced underdevelopment (Figure 5). The MRI examination identified growth-inhibited embryos that were later confirmed as *Morg1*^{-/-}. The average embryonic cavity size of *Morg1*^{-/-} mice was about 76% reduced compared to the wild-type and heterozygous animals at E8.5. *Morg1*^{-/-} embryos were also extremely small compared to average wild-type embryos and at least one day behind the physiological developmental stage. With this MRI resolution, no specific structures but just a relatively thin tissue layer was visible in the uterine cavity of *Morg1*^{-/-} embryos, whereas in the *Morg1*^{+/+}, a dorsal bending of the neuroepithelium to form the neural folds could be clearly observed (own observations). Embryos, which were first analyzed by MRI, were fixed, embedded in paraffin and subjected to IHC analysis. H&E staining confirmed the developmental delay in mutants (Figure 5A). *Morg1*^{+/+} embryos exhibited around eight pairs of somites, an optic vesicle, a thick and uniform neuroepithelium and development of the heart, with cardiac looping of the linear heart tube. *Morg1*^{-/-} embryos lacked most of these developmental features. Their neuroepithelium was still thin and irregular. The head region was underdeveloped with no discernible head fold and neither a cardiac primordium nor somites were recognizable in the section. Furthermore, mutants had a clearly smaller cell mass and cell density and their embryonic tissue showed anomalous organization and showed failure of chorioallantoic fusion.

3.6. Severe Placental Abnormalities and Delayed Neural Tube Closure in Morg1^{-/-} Embryos

Early embryonic lethality between E9.5 and E14.5 is commonly associated with placental malformations that lead to undersupply and cause maldevelopment. In a study of 103 embryonic lethal and subviable (strains in which the proportion of mutant offspring is >0% but ≤13%) knockout lines, 68% of the lines that were lethal at or after mid-gestation showed placental dysmorphologies [19]. Proper placental vascularization is essential for the physiological development of the embryo and surrounding tissues [23]. Embryonic malformations showing significant statistical correlation with placental defects included abnormalities in the heart, brain and vascular system. Effects of placental insufficiency on brain development manifested especially in the forebrain [19]. The embryonic trophoblast is essential for implantation and interacts with the maternal uterus. Trophoblast giant cells (TGC) initially make contact with the uterine cell lining and invade the uterine tissue [24]. Therefore, the invasion of vessels around the chorionic plate and labyrinth layer and the development of the TGC layer were investigated (Figures 4E and 5B). In *Morg1*^{-/-} embryos on E8.5, a severe impairment of placental vascularization was observed. In the wild-type placenta, the maturing labyrinth layer already contained numerous vascular beds full of erythrocytes, which were lacking in the *Morg1*^{-/-} (Figure 5B).

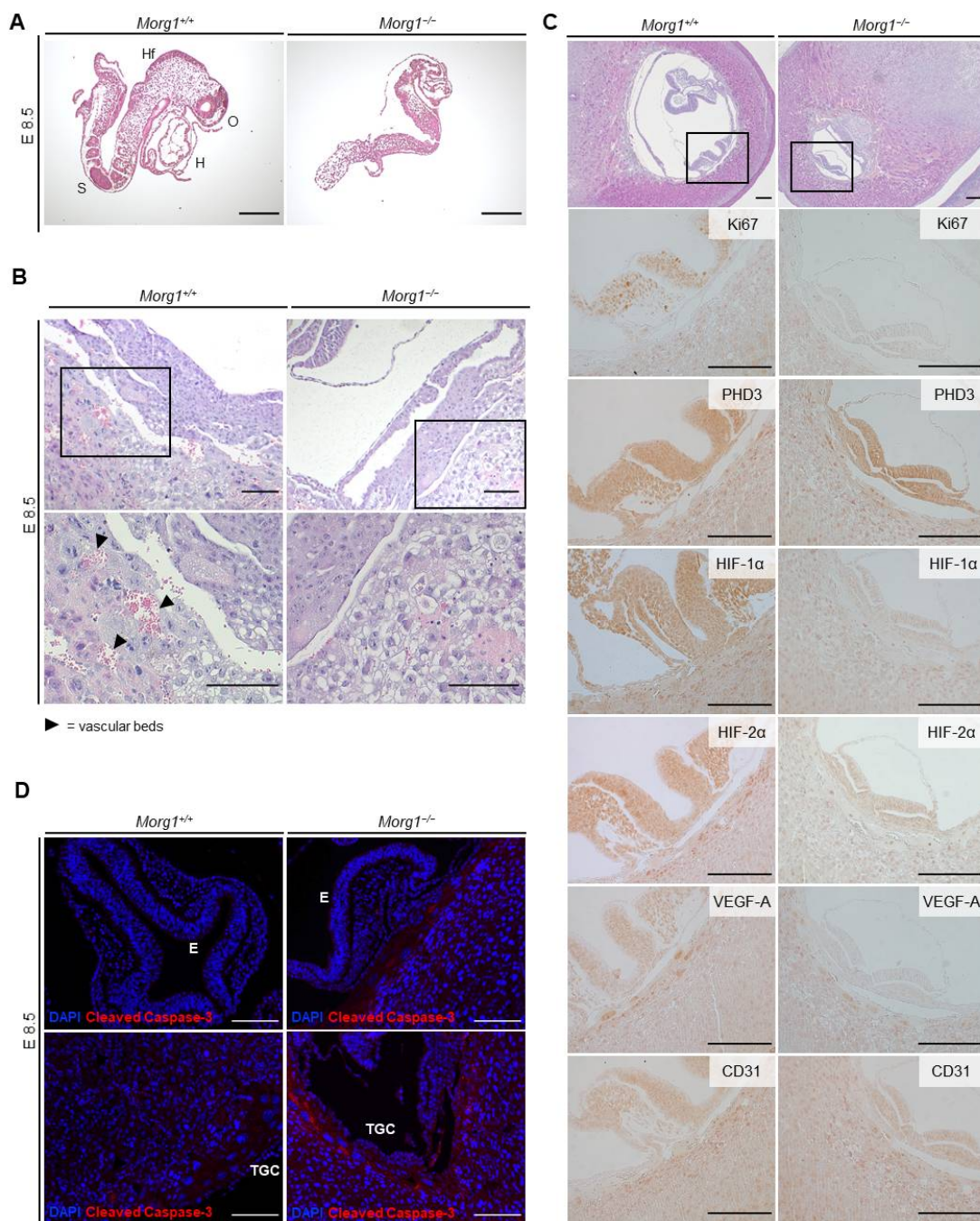


Figure 5. Maldevelopment of *Morg1* knockout embryo on E8.5 and impaired vascularization through aberrant levels of HIF-1 α , HIF-2 α , VEGF-A, Ki67 and cleaved caspase 3 on E8.5. E = embryonic day; H = heart; HF = head fold; MRI = magnetic resonance imaging; O = optic vesicle; S = somites; TGC = trophoblast giant cell. Scale bar = 200 μ m. (A) H&E staining of *Morg1*^{+/+} and *Morg1*^{-/-} embryos on E8.5 of the same litter after preparation. The underdeveloped *Morg1*^{-/-} embryos lack organ primordia and shows failure in chorioallantoic fusion. (B) H&E staining of extraembryonic tissue. *Morg1*^{-/-} placenta exhibits extended layer of TGCs and shows impaired vascularization including diminished formation of vascular beds. N = 6. (C) H&E and IHC staining of *Morg1*^{+/+} and *Morg1*^{-/-} embryo and extraembryonic tissue. *Morg1*^{-/-} embryo exhibits impaired formation and development of neural tube and diminished expression of HIF-1 α , HIF-2 α , VEGF-A and Ki67. N = 5 each of wild-type and knockout with qualitatively similar stainings. (D) Representative immunofluorescence staining of *Morg1*^{+/+} and *Morg1*^{-/-} embryo. TGCs surrounding the *Morg1*^{-/-} embryo show elevated levels of activated caspase-3. N = 5 each of wild-type and knockout with qualitatively similar staining.

To demonstrate an impact of Morg1 depletion on the developmental stage of the embryo, the tissue-specific expression pattern of key markers that both influence embryonic development and are associated with MORG1 manifestations was examined (Figure 5C). E8.5 Morg1^{-/-} and Morg1^{+/+} embryos of the same litter were cut in sequence and the plane at which the neural tube was transversely sectioned was chosen for evaluation, because the development from the neural plate to the closed neural tube takes a crucial step at this time and serves as an indicator of physiological growth (Figure 5C, area marked with rectangle in top H&E images). The size of the uterus itself was not different, but the embryonic cavity of Morg1^{-/-} embryos was significantly smaller. The thickness of the mutant neuroepithelium was reduced by about half and the neural groove was less advanced than in the Morg1^{+/+}, indicating developmental delay. Failure of neural tube closure was uniformly observed in several Morg1^{-/-} embryos. The process of neural tube morphogenesis is highly complex and apicobasal polarity mechanisms play a major role in neural tube closure [25]. The study of Hayase et al. showed that MORG1 is involved in the formation of cell polarization in epithelial cells. The formation of apicobasal polarity in epithelial cells involves atypical protein kinase C (aPKC), which constitutively interacts with Par6, an evolutionarily conserved adaptor protein [8]. The Par6-aPKC complex is shown to translocate from the cytoplasm to the apical membrane, where the complex may be anchored with the apical membrane-integrated protein Crumbs3 (Crb3), which is reinforced with the apically localized small GTPase Cdc42 in the GTP-bound form [8]. For many years, the mechanism for Par6-aPKC translocation to the apical membrane was unclear, but then, it was shown that the forced targeting of the complex to the apical surface is mediated by MORG1 [8]. This conclusion is based on the findings that MORG1 directly binds not only to Par6 but also to Crb3, which facilitates Par6 binding to Crb3, leading to apical targeting of Par6-aPKC [8].

To ensure rapid growth during this phase of embryogenesis, a high proliferation rate in embryonic tissue is indispensable. In the wild-type embryos, a high expression level of Ki67 was detected in all embryonic tissues and especially in the neural tube (Figure 5C), which is typical around E8 [26]. In contrast to E12.5, where Ki67-positive cells were now restricted to only a thin layer of neuroepithelium (Figure 2B), they were distributed throughout the neuroepithelium at day E8.5 (Figure 5C). MORG1 expression was also uniformly distributed in the neuroepithelium in wild-type at E8.5, which did not change at days E9.5 and E10.5 (own observations). In Morg1^{-/-} embryos at E8.5, the proliferation rate decreased considerably and only very few cells were positive for Ki67, indicating stagnant proliferation and development. Thus, it is reasonable to assume that cell cycle arrest occurred in most cells of the embryonic tissue at that stage and that further development and progression came to a standstill.

Because a known role of MORG1 is to stabilize PHD3 and increase oxygen-dependent degradation of HIF, we examined the expressions of PHD3 and HIF-1 α and -2 α . Although PHD3 was not affected by knockout of Morg1, lower levels of both HIF α isoforms were present in Morg1^{-/-} embryos and extraembryonic tissues (Figure 5C). Former nephrological studies with adult mice did show that in heterozygous Morg1 mutants, a loss of PHD3 stabilization leads to reduced PHD3 concentration and, therefore, reduced HIF α degradation [7], but this was not comparable to the present study. Apart from the fact that this study examined adult kidney tissue from Morg1^{+/-} mice and early embryonic stages in homozygous knockout, there are other PHDs besides PHD3, namely PHD1 and 2, that regulate the stability of HIF α subunits. In any case, during embryonic development, other biological functions of MORG1 seem to play a role rather than that of being a scaffolding protein of PHD3. An influence of MAPK signaling pathway on HIF expression came into focus as a possible factor, because a requirement of the ERK-pathway for HIF-1 induction was described in neurons and a direct phosphorylation of HIF-1 by ERK 1/2, leading to an increased half-life, was reported [27,28]. Since MAP kinases are essential for neuronal migration during brain development [29,30], a disruption of proper MAP kinase function by deletion of the scaffolding protein MORG1 may easily explain the severe neuronal devel-

opment defects. For example, disruption of the ERK2 gene leads to impaired trophoblast development and post-implantation lethality [31] and knockout of MEK1 causes embryonic death on E10.5 due to impaired vascularization in the labyrinth layer of the placenta [32]. The observed phenotypic changes of *Morg1* knockout offspring appear to manifest similarly to suppressions of downstream signaling molecules of the MAPK pathway.

Coming back to the role of HIF, before the onset of placental circulation around E8/E9, the embryos reside in a hypoxic environment and both HIF-1 α /2 α are expressed at high levels [33]. Beyond this time point, the expression of HIF-1 α and HIF-2 α vary widely depending on tissue and time point of gestation. However, the exact reason for the divergent expression patterns remains unclear to date [34,35]. The reported phenotypes of HIF-1 α and/or HIF-2 α knockout embryos fit largely with the observations of the *Morg1*^{-/-} embryos reported here. HIF knockout embryos showed angiogenic and neural tube defects and cardiovascular malformations, and they underwent developmental arrest by E9 and lethality by E10.5 [36]. Furthermore, the placenta of a double knockout of HIF-1 α and -2 α exhibited no fetal blood vessels, expanded TGC numbers and aberrant placental architecture [36], proving the importance of HIF on proliferation, survival and differentiation of multiple embryonic tissues.

VEGF-A is essential for embryonic and placental development due to its major role during hematopoiesis, vascularization and angiogenesis [37]. During murine embryogenesis, it can be detected from E7 in the extraembryonic and embryonic ectoderm. By E8.5, VEGF-A is present especially in the trophoblast surrounding the embryo, the embryonic myocardium, gut endoderm, embryonic mesenchyme and amniotic ectoderm and, later, in the neuroectoderm of the head [38]. In accordance with these literature data, on E8.5, VEGF-A was highly expressed in the *Morg1*^{+/+} trophoblast surrounding the embryo and the embryo itself (Figure 5C). The *Morg1*^{-/-} embryos lacked VEGF-A expression and the staining of the trophoblast cells was less intense than in the wild-type. Previous studies indicated that HIF-1 α is involved in mediating VEGF transcriptional activation in hypoxic cells [34].

In conclusion, the reduced expression of VEGF-A, HIF-1 α and HIF-2 α symptomatically matched the impaired vascularization of the placenta and very likely played a role in the progression of embryonic malformation. Proliferative arrest preceded subsequent apoptosis and decomposition of the embryo. Since hardly any proliferating cells were present on E8.5, it can be assumed that undersupply was previously relevant in underdevelopment.

CD31, widely used as an endothelial cell marker, indicates the presence of vascularization and angiogenesis [39]. Both genotypes showed the same expression of CD31 in intensity and localization (Figure 5C). Expression appeared in the embryo itself and all surrounding tissues including trophoblastic layer and decidua. Thus, we concluded that impaired expression of CD31 was not a likely cause for the insufficient formation of vessels in *Morg1*^{-/-} embryos.

Embryonic and extraembryonic tissues undergo constant remodeling, which is not possible without expression of proliferative and apoptotic markers [40]. Cleaved caspase-3 represents a reliable marker for early detection of apoptotic cells because it is responsible for most of the proteolysis during apoptotic processes and activated during the intrinsic and extrinsic apoptosis signaling pathway [41]. Immunofluorescence antibody staining for cleaved caspase-3 of the embryo itself and the layer of TGCs surrounding the embryonic vesicle are shown in Figure 5D. In the *Morg1*^{+/+} embryos on E8.5, no cleaved caspase-3 positive cell could be identified. When examining the *Morg1*^{-/-} embryos, approximately one caspase-expressing cell was found per section, showing no unphysiological signs. However, strong activation of caspase-3 was observed in the *Morg1*^{-/-} trophoblastic layer. Even if there were no signs of cell death in the embryos, there already seemed to be strong deviations from the *Morg1*^{+/+} in the TGC. Advanced apoptosis from E9.5 could be identified in the H&E staining (Figure 4B), as described previously.

Taking all findings together, we document here that the intrauterine death of *Morg1*^{-/-} embryos is most likely caused by a severe failure to develop brain and other neuronal structures such as the spinal cord and ganglia. The pivotal event of the central nervous

system, namely the formation and closure of the anterior neuropore, normally occurs at day E9.0 [42]. We previously found that MORG1 is expressed in the normal human brain and is downregulated following ischemic brain damage [43]. However, MORG1 expression was high in reactive astrocytes adjacent to the ischemic brain areas [43]. Furthermore, in an experimental model of brain ischemia (MCAO), a comparison of *Morg1*^{+/-} mice to the wild-type revealed a significantly reduced infarct volume despite a similar restriction of blood flow in both mice phenotypes as measured by laser Doppler flowmetry [44]. These findings clearly point to a central role of MORG1 in astrocyte and/or neuronal development and remodeling.

4. Conclusions

In summary, *Morg1*^{-/-} embryos on E8.5 and E9.5 showed failure to turn, defective chorioallantoic fusion, growth inhibition, maldevelopment, very low cell mass, poorly differentiated tissue, impaired vascularization and heart development and a particularly thin and irregular neuroepithelium of the underdeveloped neural tube. Given the regulatory role of MORG1 on the HIF and MAPK pathways as well as of apicobasal polarity mechanisms, and since these were shown to play a critical role in embryonic development, disruption of these pathways is likely to be causally involved. Maldevelopment of the surrounding extraembryonic tissue may further lead to an undersupply of the *Morg1*^{-/-} embryo, which is reflected by proliferative arrest on E8.5. The presented results underpin a major role of MORG1 in nervous system development. Thus, and given the multifaceted molecular biological influence and wide expression of MORG1, it is reasonable to speak of a multifactorial process that causes embryonic death in mutant mice. More extensive studies, especially to changes in ERK phosphorylation/nuclear translocation and the polarization of neuroepithelial cells in the homozygous *Morg1* knockout, are needed to further analyze the influence of MORG1 during mammalian embryonic development and its crosstalk with placental tissue.

Supplementary Materials: The following supporting information can be downloaded at: <https://www.mdpi.com/article/10.3390/biom13071037/s1>, Figure S1. Control stains to assess the specificity of the antibody MORG1. (A) Representative image of “negative tissue” control on MORG1 knockout embryos. (B) Representative images of “secondary antibody only” and “isotype” control (IgG) on wildtype embryos and adult tissues. (C) Autofluorescence control of the mIFs on wildtype embryos. Scale bars = 500 μ m. Figure S2. Spatiotemporal MORG1 transcription pattern of post-implantation mouse embryos generated by Geo-seq as annotated on the eGastrulation repository (<http://egastrulation.sibcb.ac.cn/aHome/>; accessed on 24 April 2023). (A) Corn plot representations of the spatial pattern of *Wdr83* gene expression at indicated embryonic stages. Each dot in the plot represents the cell sample at the specific positional address, gene expression is color-coded as computed from the transcript counts in the RNA-seq dataset. Solid circles, epiblast–ectoderm; black outlined rhombus, mesoderm; black outlined circles, endoderm; grey hollow circles, no sample. (B) Schematic illustration of the Geo-seq procedure. A, anterior; P, posterior; L, left lateral; R, right lateral; L1, anterior left lateral; R1, anterior right lateral; L2, posterior left lateral; R2, posterior right lateral; Epi1 and Epi2, divided epiblast; M, whole mesoderm; MA, anterior mesoderm; MP, posterior mesoderm; En1 and En2, divided endoderm; EA, anterior endoderm; EP, posterior endoderm. For more details see references [45–47].

Author Contributions: Conceptualization, I.L. and G.W.; data curation, I.L.; formal analysis, S.W., L.M., A.U., C.L., I.L. and G.W.; funding acquisition, A.U.; investigation, S.W., L.M., K.-H.H., M.S.-C., A.U. and I.L.; methodology, K.-H.H. and A.B.; project administration, I.L. and G.W.; supervision, I.L.; validation, S.W. and I.L.; visualization, S.W. and I.L.; writing—original draft, S.W. and I.L.; writing—review and editing, K.-H.H., L.M., M.S.-C., A.U., C.L., A.B., I.L. and G.W. All authors have read and agreed to the published version of the manuscript.

Funding: A.U. received funding from IZKF Jena Advanced Medical Scientist program (AMSP06).

Institutional Review Board Statement: The animal study protocol was approved by the Ethics Committee of Landesamt für Gesundheit und Verbraucherschutz Hamburg.

Informed Consent Statement: Not applicable.

Data Availability Statement: Not applicable.

Acknowledgments: We would like to acknowledge the allocation of equipment infrastructure at mIF and whole slide scanning by the Pathology Section, University Hospital Jena. We thank Ulrike Hopfer (now Roche, Basel, Switzerland) for constructing the initial targeting vector. Furthermore, we thank Nadja Ziller, Simone Schönfelder, Simone Goebel and Dagmar Samsel for the technical support. Many thanks to Karin Elflein for helpful discussions as well as Ignacio Rubio for critical reading of the manuscript.

Conflicts of Interest: The authors declare no conflict of interest.

References

1. Xu, C.; Min, J. Structure and function of WD40 domain proteins. *Protein Cell* **2011**, *2*, 202–214. [[CrossRef](#)]
2. Vomastek, T.; Schaeffer, H.J.; Tarcsafalvi, A.; Smolkin, M.E.; Bissonette, E.A.; Weber, M.J. Modular construction of a signaling scaffold: MORG1 interacts with components of the ERK cascade and links ERK signaling to specific agonists. *Proc. Natl. Acad. Sci. USA* **2004**, *101*, 6981–6986. [[CrossRef](#)]
3. Teis, D.; Taub, N.; Kurzbauer, R.; Hilber, D.; de Araujo, M.E.; Erlacher, M.; Offterdinger, M.; Villunger, A.; Geley, S.; Bohn, G.; et al. p14-MP1-MEK1 signaling regulates endosomal traffic and cellular proliferation during tissue homeostasis. *J. Cell Biol.* **2006**, *175*, 861–868. [[CrossRef](#)]
4. Albadari, N.; Deng, S.; Li, W. The transcriptional factors HIF-1 and HIF-2 and their novel inhibitors in cancer therapy. *Expert Opin. Drug Discov.* **2019**, *14*, 667–682. [[CrossRef](#)]
5. Lee, J.W.; Ko, J.; Ju, C.; Eltzschig, H.K. Hypoxia signaling in human diseases and therapeutic targets. *Exp. Mol. Med.* **2019**, *51*, 1–13. [[CrossRef](#)]
6. Loeffler, I.; Wolf, G. Morg1 heterozygous deficiency ameliorates hypoxia-induced acute renal injury. *Am. J. Physiol. Renal. Physiol.* **2015**, *308*, F511–F521. [[CrossRef](#)]
7. Hopfer, U.; Hopfer, H.; Jablonski, K.; Stahl, R.A.; Wolf, G. The novel WD-repeat protein Morg1 acts as a molecular scaffold for hypoxia-inducible factor prolyl hydroxylase 3 (PHD3). *J. Biol. Chem.* **2006**, *281*, 8645–8655. [[CrossRef](#)]
8. Hayase, J.; Kamakura, S.; Iwakiri, Y.; Yamaguchi, Y.; Izaki, T.; Ito, T.; Sumimoto, H. The WD40 protein Morg1 facilitates Par6-aPKC binding to Crb3 for apical identity in epithelial cells. *J. Cell Biol.* **2013**, *200*, 635–650. [[CrossRef](#)]
9. Rappel, W.J.; Edelstein-Keshet, L. Mechanisms of Cell Polarization. *Curr. Opin. Syst. Biol.* **2017**, *3*, 43–53. [[CrossRef](#)]
10. Loeffler, I.; Wolf, G. MORG1 (Mitogen-Activated Protein Kinase Organizer 1). In *Encyclopedia of Signaling Molecules*; Choi, S., Ed.; Springer International Publishing: Berlin/Heidelberg, Germany, 2018; p. 6060.
11. Hammerschmidt, E.; Loeffler, I.; Wolf, G. Morg1 heterozygous mice are protected from acute renal ischemia-reperfusion injury. *Am. J. Physiol. Renal. Physiol.* **2009**, *297*, F1273–F1287. [[CrossRef](#)]
12. Loeffler, I.; Liebisch, M.; Daniel, C.; Amann, K.; Wolf, G. Heterozygosity of mitogen-activated protein kinase organizer 1 ameliorates diabetic nephropathy and suppresses epithelial-to-mesenchymal transition-like changes in db/db mice. *Nephrol. Dial. Transplant.* **2017**, *32*, 2017–2034. [[CrossRef](#)]
13. Jankowski, E.; Wulf, S.; Ziller, N.; Wolf, G.; Loeffler, I. MORG1-A Negative Modulator of Renal Lipid Metabolism in Murine Diabetes. *Biomedicines* **2021**, *10*, 30. [[CrossRef](#)]
14. Herrmann, K.H.; Hung, L.Y.; Reichenbach, J.R. Fast 3D Isotropic High-Resolution MRI of Mouse Brain Using a Variable Flip Angle RARE Sequence with T2 Compensation @9. 4T. In Proceedings of the 30th Annual Meeting ISMRM, London, UK, 7–12 May 2022.
15. Sun, X.; Kaufman, P.D. Ki-67: More than a proliferation marker. *Chromosoma* **2018**, *127*, 175–186. [[CrossRef](#)]
16. Wilm, B.; Muñoz-Chapuli, R. The Role of WT1 in Embryonic Development and Normal Organ Homeostasis. *Methods Mol. Biol.* **2016**, *1467*, 23–39. [[CrossRef](#)]
17. Capecchi, M.R. Altering the genome by homologous recombination. *Science* **1989**, *244*, 1288–1292. [[CrossRef](#)]
18. Friedel, R.H.; Wurst, W.; Wefers, B.; Kuhn, R. Generating conditional knockout mice. *Methods Mol. Biol.* **2011**, *693*, 205–231. [[CrossRef](#)]
19. Perez-Garcia, V.; Fineberg, E.; Wilson, R.; Murray, A.; Mazzeo, C.I.; Tudor, C.; Sienerth, A.; White, J.K.; Tuck, E.; Ryder, E.J.; et al. Placentation defects are highly prevalent in embryonic lethal mouse mutants. *Nature* **2018**, *555*, 463–468. [[CrossRef](#)]
20. Papaioannou, V.E.; Behringer, R.R. Early embryonic lethality in genetically engineered mice: Diagnosis and phenotypic analysis. *Vet. Pathol.* **2012**, *49*, 64–70. [[CrossRef](#)]
21. Stumpo, D.J.; Byrd, N.A.; Phillips, R.S.; Ghosh, S.; Maronpot, R.R.; Castranio, T.; Meyers, E.N.; Mishina, Y.; Blackshear, P.J. Chorioallantoic fusion defects and embryonic lethality resulting from disruption of Zfp36L1, a gene encoding a CCCH tandem zinc finger protein of the Tristetraprolin family. *Mol. Cell Biol.* **2004**, *24*, 6445–6455. [[CrossRef](#)]
22. Morin-Kensicki, E.M.; Boone, B.N.; Howell, M.; Stonebraker, J.R.; Teed, J.; Alb, J.G.; Magnuson, T.R.; O’Neal, W.; Milgram, S.L. Defects in yolk sac vasculogenesis, chorioallantoic fusion, and embryonic axis elongation in mice with targeted disruption of Yap65. *Mol. Cell Biol.* **2006**, *26*, 77–87. [[CrossRef](#)]
23. Rada, C.C.; Murray, G.; England, S.K. The SK3 channel promotes placental vascularization by enhancing secretion of angiogenic factors. *Am. J. Physiol. Endocrinol. Metab.* **2014**, *307*, E935–E943. [[CrossRef](#)]

24. Hemberger, M.; Hanna, C.W.; Dean, W. Mechanisms of early placental development in mouse and humans. *Nat. Rev. Genet.* **2020**, *21*, 27–43. [[CrossRef](#)]
25. Eom, D.S.; Amarnath, S.; Agarwala, S. Apicobasal polarity and neural tube closure. *Dev. Growth Differ.* **2013**, *55*, 164–172. [[CrossRef](#)]
26. Hohenstein, P.; Kielman, M.F.; Breukel, C.; Bennett, L.M.; Wiseman, R.; Krimpenfort, P.; Cornelisse, C.; van Ommen, G.J.; Devilee, P.; Fodde, R. A targeted mouse Brca1 mutation removing the last BRCT repeat results in apoptosis and embryonic lethality at the headfold stage. *Oncogene* **2001**, *20*, 2544–2550. [[CrossRef](#)]
27. Chu, C.T.; Levinthal, D.J.; Kulich, S.M.; Chalovich, E.M.; DeFranco, D.B. Oxidative neuronal injury. The dark side of ERK1/2. *Eur. J. Biochem.* **2004**, *271*, 2060–2066. [[CrossRef](#)]
28. Hofer, T.; Desbaillets, I.; Hopfl, G.; Gassmann, M.; Wenger, R.H. Dissecting hypoxia-dependent and hypoxia-independent steps in the HIF-1alpha activation cascade: Implications for HIF-1alpha gene therapy. *FASEB J.* **2001**, *15*, 2715–2717. [[CrossRef](#)]
29. Ayala, R.; Shu, T.; Tsai, L.H. Trekking across the brain: The journey of neuronal migration. *Cell* **2007**, *128*, 29–43. [[CrossRef](#)]
30. Scholzke, M.N.; Schwaninger, M. Transcriptional regulation of neurogenesis: Potential mechanisms in cerebral ischemia. *J. Mol. Med.* **2007**, *85*, 577–588. [[CrossRef](#)]
31. Saba-El-Leil, M.K.; Vella, F.D.; Vernay, B.; Voisin, L.; Chen, L.; Labrecque, N.; Ang, S.L.; Meloche, S. An essential function of the mitogen-activated protein kinase Erk2 in mouse trophoblast development. *EMBO Rep.* **2003**, *4*, 964–968. [[CrossRef](#)]
32. Giroux, S.; Tremblay, M.; Bernard, D.; Cardin-Girard, J.F.; Aubry, S.; Larouche, L.; Rousseau, S.; Huot, J.; Landry, J.; Jeannotte, L.; et al. Embryonic death of Mek1-deficient mice reveals a role for this kinase in angiogenesis in the labyrinthine region of the placenta. *Curr. Biol.* **1999**, *9*, 369–372. [[CrossRef](#)]
33. Adelman, D.M.; Gertsenstein, M.; Nagy, A.; Simon, M.C.; Maltepe, E. Placental cell fates are regulated in vivo by HIF-mediated hypoxia responses. *Genes Dev.* **2000**, *14*, 3191–3203. [[CrossRef](#)]
34. Iyer, N.V.; Kotch, L.E.; Agani, F.; Leung, S.W.; Laughner, E.; Wenger, R.H.; Gassmann, M.; Gearhart, J.D.; Lawler, A.M.; Yu, A.Y.; et al. Cellular and developmental control of O₂ homeostasis by hypoxia-inducible factor 1 alpha. *Genes Dev.* **1998**, *12*, 149–162. [[CrossRef](#)]
35. Rojas, D.A.; Perez-Munizaga, D.A.; Centanin, L.; Antonelli, M.; Wappner, P.; Allende, M.L.; Reyes, A.E. Cloning of hif-1alpha and hif-2alpha and mRNA expression pattern during development in zebrafish. *Gene Expr. Patterns* **2007**, *7*, 339–345. [[CrossRef](#)]
36. Cowden Dahl, K.D.; Fryer, B.H.; Mack, F.A.; Comperolle, V.; Maltepe, E.; Adelman, D.M.; Carmeliet, P.; Simon, M.C. Hypoxia-inducible factors 1alpha and 2alpha regulate trophoblast differentiation. *Mol. Cell Biol.* **2005**, *25*, 10479–10491. [[CrossRef](#)]
37. Shibuya, M. Vascular Endothelial Growth Factor (VEGF) and Its Receptor (VEGFR) Signaling in Angiogenesis: A Crucial Target for Anti- and Pro-Angiogenic Therapies. *Genes Cancer* **2011**, *2*, 1097–1105. [[CrossRef](#)]
38. Holmes, D.I.; Zachary, I. The vascular endothelial growth factor (VEGF) family: Angiogenic factors in health and disease. *Genome Biol.* **2005**, *6*, 209. [[CrossRef](#)]
39. Jiang, L.; Lin, L.; Li, R.; Yuan, C.; Xu, M.; Huang, J.H.; Huang, M. Dimer conformation of soluble PECAM-1, an endothelial marker. *Int. J. Biochem. Cell Biol.* **2016**, *77*, 102–108. [[CrossRef](#)]
40. Ali-Khan, S.E.; Hales, B.F. Caspase-3 mediates retinoid-induced apoptosis in the organogenesis-stage mouse limb. *Birth Defects Res. A Clin. Mol. Teratol.* **2003**, *67*, 848–860. [[CrossRef](#)]
41. Crowley, L.C.; Waterhouse, N.J. Detecting Cleaved Caspase-3 in Apoptotic Cells by Flow Cytometry. *Cold Spring Harb. Protoc.* **2016**, *2016*, pdb-prot087312. [[CrossRef](#)]
42. Theiler, K. *The House Mouse: Atlas of Embryonic Development*; Springer: Berlin/Heidelberg, Germany, 1989.
43. Haase, D.; Keiner, S.; Mawrin, C.; Wolf, G. Reduced Morg1 expression in ischemic human brain. *Neurosci. Lett.* **2009**, *455*, 46–50. [[CrossRef](#)]
44. Stahr, A.; Frahm, C.; Kretz, A.; Bondeva, T.; Witte, O.W.; Wolf, G. Morg1(+/-) heterozygous mice are protected from experimentally induced focal cerebral ischemia. *Brain Res.* **2012**, *1482*, 22–31. [[CrossRef](#)]
45. Peng, G.; Suo, S.; Cui, G.; Yu, F.; Wang, R.; Chen, J.; Chen, S.; Liu, Z.; Chen, G.; Qian, Y.; et al. Molecular architecture of lineage allocation and tissue organization in early mouse embryo. *Nature* **2019**, *572*, 528–532. [[CrossRef](#)]
46. Peng, G.; Suo, S.; Chen, J.; Chen, W.; Liu, C.; Yu, F.; Wang, R.; Chen, S.; Sun, N.; Cui, G.; et al. Spatial Transcriptome for the Molecular Annotation of Lineage Fates and Cell Identity in Mid-gastrula Mouse Embryo. *Dev. Cell* **2020**, *55*, 802–804. [[CrossRef](#)]
47. Chen, J.; Suo, S.; Tam, P.P.; Han, J.J.; Peng, G.; Jing, N. Spatial transcriptomic analysis of cryosectioned tissue samples with Geo-seq. *Nat. Protoc.* **2017**, *12*, 566–580. [[CrossRef](#)]

Disclaimer/Publisher's Note: The statements, opinions and data contained in all publications are solely those of the individual author(s) and contributor(s) and not of MDPI and/or the editor(s). MDPI and/or the editor(s) disclaim responsibility for any injury to people or property resulting from any ideas, methods, instructions or products referred to in the content.